The Impact of Topography on the Initial Error Growth Associated with Moist Convection

Pin-Ying Wu and Tetsuya Takemi
Disaster Prevention Research Institute, Kyoto University, Kyoto, Japan

Abstract

Identical twin experiments with and without topography are conducted with the Weather Research and Forecasting (WRF) model in an idealized framework to investigate the impact of topography on the initial error growth associated with moist convection. A topography is set as a single Gaussian shape mountain with a peak height of about 1000 m. Both experiments show clear diurnal cycles, while moist convection develops earlier and organizes to a larger size in the experiment with topography. To evaluate the initial error growth, a metric referred to as moist difference total energy (MDTE) is proposed to represent the differences between the two simulations in twin experiments. The horizontal spatial distribution, temporal evolution, and horizontal wavenumber space of the MDTE suggest that the error growth is greatly dominated by the different features of convection development between the two experiments. The analysis based on individual cloud areas shows that the convective clouds developing over the mountain have smaller MDTE at the early stage of development.

(**Citation**: Wu, P.-Y., and T. Takemi, 2021: The impact of topography on the initial error growth associated with moist convection. *SOLA*, **17**, 134−139, doi:10.2151/sola.2021-024.)

1. Introduction

Rapidly developing moist convection such as afternoon thunderstorms could bring sudden heavy rainfall and lead to disasters like flooding and landslides. Afternoon thunderstorms often develop over mountain areas and sometimes cause heavy rainfall in nearby cities (e.g., Jou 1994; Lin et al. 2011). Mountain topography could decrease the degree of freedom of the atmosphere by providing a stationary, steady-state forcing (Carbone et al. 2002; Houze 2012). While the predictability of moist convection is limited by the rapid error growth dominated by the nonlinear moist processes in it (e.g., Zhang et al. 2003; Selz and Craig 2015), the topography may increase the predictability. From a practical perspective, Bachmann et al. (2019, 2020) indicated that orography increases the predictability of precipitation. On the other hand, although the intrinsic predictability and the initial error growth (Supplement 1) at different scales have been widely investigated (e.g., Ngan and Eperon 2011; Sun and Zhang 2016; Weyn and Durran 2017; Judt 2018), the number of studies focusing on the impact of topography is still limited. Does the forcing of topography decrease the nonlinearity in rapidly developing moist convection and its associated initial error growth rate? Understanding the effects of topography on the predictability of moist convection is expected to help us provide better numerical prediction of weather over mountainous areas.

This study focuses on the moist convection resulting from convective instability under synoptically undisturbed conditions, like afternoon thunderstorms. We conduct idealized numerical simulations and identical twin experiments (e.g., Zhang et al. 2007; Bierdel et al. 2018) with and without topography to investigate the topographic effects on the initial error growth during the development of moist convection. The model configuration and the experimental design are described in Section 2. The results of experiments with and without topography are provided in Section 3, and Section 4 presents the summary.

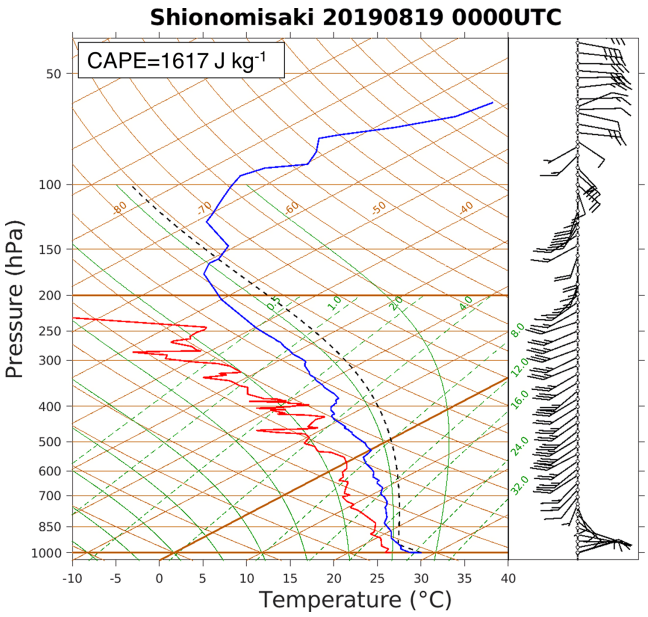

Fig. 1. The sounding data from the station at Shionomisaki, Wakayama, Japan at 0900 JST (0000 UCT) on 19 August 2019. The blue and red curves show the profile of temperature and dew point temperature, respectively. The wind barbs on the right show the profile of wind direction and speed (each short barb represents 5 knots).

2. Methodology

This study uses the Advanced Research WRF model version 4.1.2 (Skamarock et al. 2019) with full physics packages. The physics parameterizations used here are described in Supplement 2. The computational domain covers the area of 300 km × 300 km × 25 km, having 50 vertical levels, at 1-km horizontal grid spacing. The lateral boundary condition is doubly periodic. For the initial vertical profile, data observed at the Shionomisaki station, Wakayama, Japan at 0900 Japan Standard Time (JST or UTC+9) on 19 August 2019 (Fig. 1) is extended horizontally homogeneous. Hence the longitude and latitude of the model are set to 135.76°E and 33.35°N, corresponding to the location of the Shionomisaki station, with the Coriolis force set to a constant value of 7.9958×10^{-5}. The land use is all wooden wetland.

Two identical twin experiments with and without topography (hereafter referred to as TOPO and FLAT, respectively) are conducted. In TOPO, a Gaussian-shaped mountain with the peak height of 993.1268 m and about 50-km width is embedded in the southwestern quadrant of the domain (Figs. 2g−2l). Both TOPO and FLAT consist of a control and a perturbed simulation. The control simulation is initialized at 0000 JST 22 June 2018, the summer solstice, by adding white noise of the potential tempera-

Corresponding author: Pin-Ying Wu, Disaster Prevention Research Institute, Kyoto University, Gokasho, Uji, Kyoto 611-0011, Japan. E-mail: wu_p@storm.dpri.kyoto-u.ac.jp.

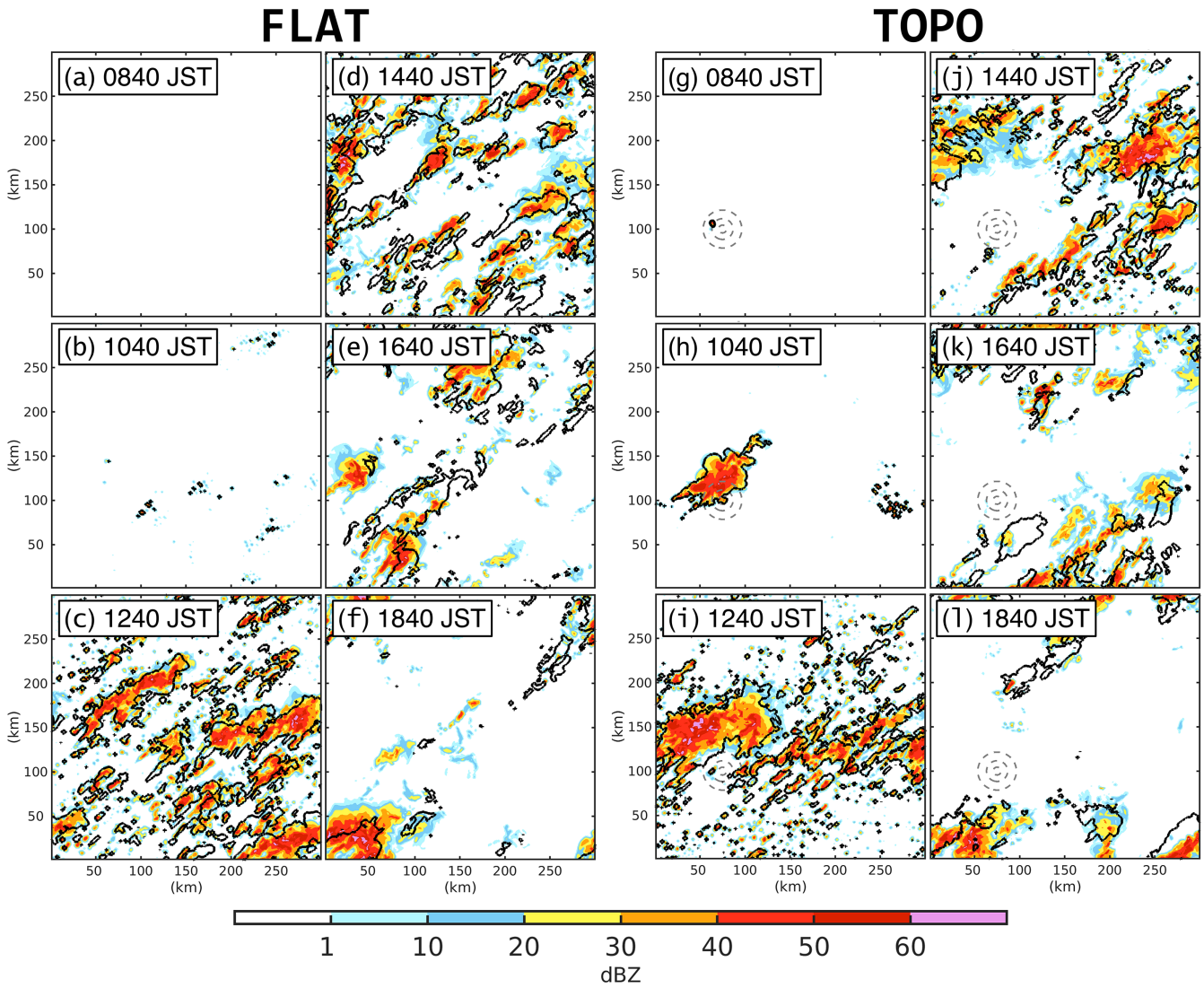

Fig. 2. The vertical maximum reflectivity calculated from the control simulation (color shaded) and the perturbed simulation (black contour; 20 dBZ) of (a)–(f) FLAT and (g)–(l) TOPO. The gray dashed contours in (g)–(l) represent the topography height equal to 100, 500, and 900 m, respectively, from the outside to the inside.

ture below 2 km with an amplitude of 0.01 K to the horizontally homogeneous initial condition. At 0600 JST 23 June, after 30-h spun up, the perturbed simulation is produced by adding Gaussian distribution random numbers with zero-mean and standard deviation equal to 0.01 g kg^{-1} to water vapor mixing ratio of the control simulation at all model grid points. As usual in the identical twin experiments, the differences between the control and perturbed simulations are regarded as the error, and its temporal and spatial variation is used to investigate the initial error growth.

To estimate the differences between the control and perturbed simulations, a metric similar to difference total energy (DTE) used in previous studies (e.g., Zhang et al. 2003; Selz and Craig 2015), but incorporating water vapor difference is proposed. We refer to it as moist DTE (MDTE), which is calculated following the equation of moist total energy norm in Ehrendorfer et al. (1999) and defined as

$$\mathrm{MDTE} = \frac{1}{2}\left[u'^2 + v'^2 + \frac{c_p}{T_r}T'^2 + \frac{L_v^2}{c_p T_r}q_v'^2 + RT_r\left(\frac{p_s'}{P_r}\right)^2\right].$$

Here, u', v', T', and q_v' are the differences of model U wind, V wind, temperature, and water vapor mixing ratio, respectively, between the two simulations at 3-dimensional grids; p_s' is the difference of surface pressure between the two simulations. T_r and P_r are the reference temperature (270 K) and reference pressure (1000 hPa), respectively, following the value used in Ehrendorfer et al. (1999); c_p, L_v, and R are the specific heat capacity at constant pressure (1004.9 J kg^{-1} K^{-1}), the latent heat of condensation (2.4359×10^6 J kg^{-1}), and the specific gas constant of dry air (287.04 J kg^{-1} K^{-1}), respectively.

3. Results

Figure 2 provides the simulated vertical maximum reflectivity (Dowell et al. 2011) from 0840 JST to 1840 JST 23 June. The development of convection in both FLAT and TOPO shows a diurnal cycle; the convection is more intensive and active at noon and dissipate in the evening. The clear diurnal cycles are also shown in the domain averaged surface-air temperature and hourly rainfall (see Supplement 3). Figure 2 also shows that the convection in TOPO starts to develop earlier and organize to a larger size over the mountain area than that in FLAT. In general, our numerical experiments successfully simulate the process of afternoon thunderstorm development. In the following, we will compare the MDTE between the control and perturbed simulations of the

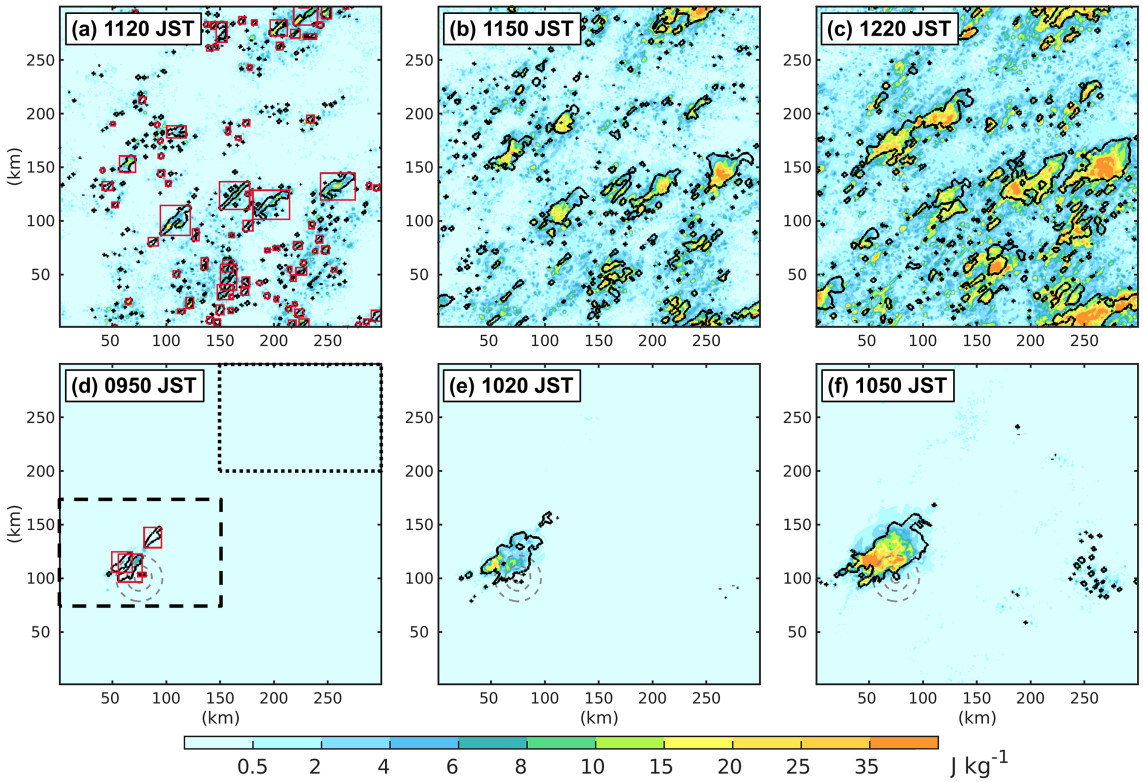

Fig. 3. The vertical mass-weighted averaged MDTE (color shaded) of (a)−(c) FLAT from 1120 JST to 1220 JST and (d)−(e) TOPO from 0950 JST to 1050 JST. The black contour shows the vertical accumulated hydrometeors (5 g kg^{-1}) of the control simulation from each experiment. The dashed-line and dotted-line boxes in (d) show the range of mountain and plain area, respectively, used for computing sub-domain average in Fig. 4. The red boxes in (a) and (d) illustrate the detected cloud areas used for producing Fig. 6.

two experiments to see how topography impacts the convection development and the associated initial error growth.

Figure 3 shows the vertical mass-weighted averaged MDTE (Nielsen and Schumacher 2016) and the vertical accumulated hydrometeors of the control simulation at some typical times of convection development for each experiment. The MDTE magnitude generally increase with time as convection develops. In particular, for both experiments, the horizontal distribution of MDTE roughly coincides with the position of convection at different times, indicating that the error growth is highly related to the moist convective process, which is also indicated in previous studies (e.g., Zhang et al. 2003).

The domination of moist convection on the error growth is also shown in the temporal evolution of MDTE. Figure 4 shows the time series of MDTE averaged over the whole domain and two sub-domains with the same size over the mountain and plain area. The mountain area is chosen to cover the convection developing over the mountain (Figs. 2g−2i), and the plain area represents the area away from the mountain. The MDTE averaged over the whole domain has a similar peak value for the two experiments, suggesting that they have similar gross MDTE over the whole computational domain. Consequently, the difference between the two experiments mainly appears as the different spatial distribution caused by the topography. This is clearly seen in the time series of MDTE averaged over the two sub-domains.

In FLAT, the temporal evolution of the error averaged over the whole domain and the two sub-domains is similar because convective clouds could occur anywhere throughout the domain in the absence of topographic forcing. In contrast, the MDTE over the two sub-domains are very different in TOPO. The MDTE over the mountain area in TOPO starts the exponential growth at the earliest time, reflecting the early development of convection caused by the mountain (Fig. 2g). It then reaches a peak slightly greater than the other peaks at 1300 JST. This is because the

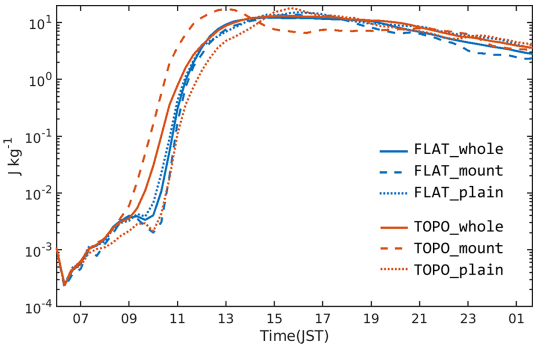

Fig. 4. Time series of the MDTE averaged over the whole domain (solid curves), mountain area (dashed curves), and plain area (dotted curves) for the experiment FLAT (blue) and TOPO (orange). The range of the mountain area and plain area are indicated in Fig. 3d.

convective clouds developing over the mountain organized to a larger size. The relationship of MDTE and convective cloud size will be further discussed later. On the other hand, the MDTE over the plain area in TOPO starts the rapid growth at a late time and has the smallest value between 1100 to 1300 JST, reflecting the lack of convection development over this area (Figs. 2h and 2i). The MDTE over the two sub-domains in TOPO exactly shows the different temporal and spatial development of convection caused by the mountain, suggesting that the impact of topography on the convection development also reflects on the temporal evolution of the initial error.

In the afternoon, the MDTE over the mountain area in TOPO decreases distinctly from 1300 to 1600 JST. At this time, the convective clouds over the mountain moved to other areas and there is

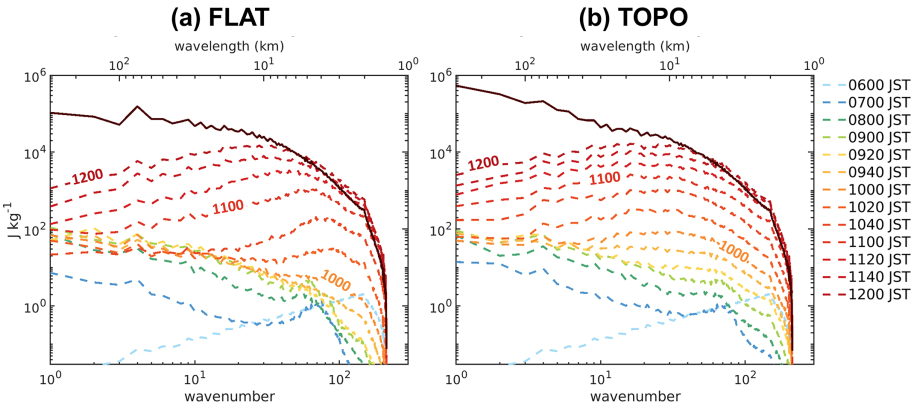

Fig. 5. Power spectra of the MDTE between the control and perturbed simulation below 10-km height (color dashed curve) for the experiment (a) FLAT and (b) TOPO. The dark red solid curve shows the power spectrum of the control simulation at 1300 JST on 23 June.

little new convection developing over the mountain (Figs. 2j−2l). The decrease of MDTE means that the distance between the control and perturbed simulation becomes closer. It implies less chaotic situation of the atmosphere at this time. In other words, although moist convection dominates the rapid growth of initial error in the morning, the decrease of MDTE in the afternoon over the mountain area demonstrates the effect of topography on decreasing the nonlinearity of the atmosphere at least when there is no moist convection.

To examine the initial error growth at different horizontal scales, we further compute power spectra (see Supplement 4) of MDTE in wavenumber space (Fig. 5). The power spectra of the control simulation at 1300 JST when the error growth reaches saturation (Fig. 4) are also plotted as a reference. During the first 3 h, the power spectra of MDTE grow at the domain scale (~100 km) and show similar features between the two experiments. From 0900 JST, they start to behave differently. In TOPO, the power spectra start to grow at about 2-km scale before 0900 JST and continue to grow at scales smaller than 50 km, pronounced at the O(10 km) scale. The spectra spread to larger scales after 1040 JST, indicating a peak at about 20 km at 1100 JST. In FLAT, on the other hand, the spectra start the growth at a late time after 0940 JST, and instead of propagating throughout the scales smaller than 50 km, they amplify at scales smaller than 10 km and have peaks at a scale corresponding to individual convective cells (~5 km) at 1100 JST.

In this way, the characteristic of the MDTE spectral growth again reflects the different temporal and spatial features of the convection development in the two experiments. Specifically, the power spectra of TOPO start to pronouncedly amplify earlier at a larger scale than those of FLAT, corresponding to the early development and larger horizontal scale of the moist convection triggered by the mountain.

In the previous discussion, we have shown that the horizontal spatial distribution (Fig. 3), temporal evolution (Fig. 4), and the horizontal wavenumber space (Fig. 5) of MDTE all reflect the features, such as initiation time and horizontal scale, of convective clouds. The experiments with and without topography show different features of MDTE because convective clouds develop differently in them. Such difference mainly highlights the topographic effect on the convection development and the predominant influences of the nonlinear moist convection on the rapid error growth. However, they provide little information about whether the mountain decreases the error growth rate triggered by the nonlinearity of the moist convective processes. For example, while the slope of the MDTE time series over the whole domain between 0900 to 1200 JST seems to be slightly shallower in TOPO than in FLAT (Fig. 4), it may only because the MDTE is smaller over the plain area due to the lack of moist convection, and not directly suggest the topographic effect on decreasing the error growth during the moist convection development.

Consequently, further analysis is desired to show whether the topography decreases the initial error growth when the moist convection is occurring, regardless of the temporal or spatial difference of the convective clouds. The idea here is to collect the results from different times and compare the MDTE associated with convective clouds of similar size. To do that, we detect individual cloud areas at different times and calculate MDTE over each could area. The cloud areas are detected by finding the horizontal contiguous regions larger than 10 grids of whose vertical accumulated hydrometeors is larger than 5 g kg^{-1} in the control simulation (i.e., black contours in Fig. 3). The detection of cloud area is illustrated by the red boxes in Figs. 3a and 3d. The area enclosed by a black contour in a red box represents an exact detected cloud area which is used to produce the following analysis.

Figure 6 shows the size of the detected cloud areas and their associated MDTE. The cloud area size is represented by the diameter of circles with the same area as the detected cloud area. The MDTE is depicted by the mean of the first 10 maximum (Figs. 6a and 6b) and the mean of all grids (Figs. 6c and 6d) of the vertical mass-weighted averaged MDTE over the detected cloud areas. The former represents the magnitude of the maximum error that a convective cloud could generate, and the latter provides the average error associated with an individual convective system.

There are some detected cloud areas having larger sizes in TOPO than in FLAT (c.f. Figs. 6a and 6b), consistent with the results of a larger convective cloud over the mountain shown in Fig. 2. In addition, the maximum magnitude of MDTE shows an increasing trend with the cloud area size (Figs. 6a and 6b), implying that some processes in a larger convective cloud, such as stronger vertical motion or rapid microphysics processes, make the extreme error greater. Thus, it is considered that the greater peak value of averaged MDTE over the mountain area of TOPO in Fig. 4 is the result of the large convective cloud like the one shown in Fig. 2i, which covers a half of the sub-domain area, and the following large extreme error generated by the strong moist convection.

At later times when the convection in FLAT starts to develop, the scatter plots between the two experiments are similar. However, the points resulted from cloud areas before 1050 JST in TOPO show smaller MDTE than others. This smaller MDTE is shown in both extreme (Fig. 6b) and averaged value (Fig. 6d). For example, for cloud areas with about 10-km size, the magnitude of extreme MDTE in FLAT are about O(10) (Fig. 6a). In contrast, the cloud areas with similar size but developing earlier at 0920 or 0950 JST in TOPO have the MDTE magnitude of only O(1) (Fig. 6b). These points correspond to the convective clouds that develop over the mountain area in the morning. For example, the 4 dark-blue points of 0950 JST in Fig. 6b are exactly the results of cloud areas illustrated in Fig. 3d. The difference between FLAT and TOPO in Fig. 6 suggests that for convective clouds with similar size, those triggered by the mountain lead to smaller MDTE at the early stage

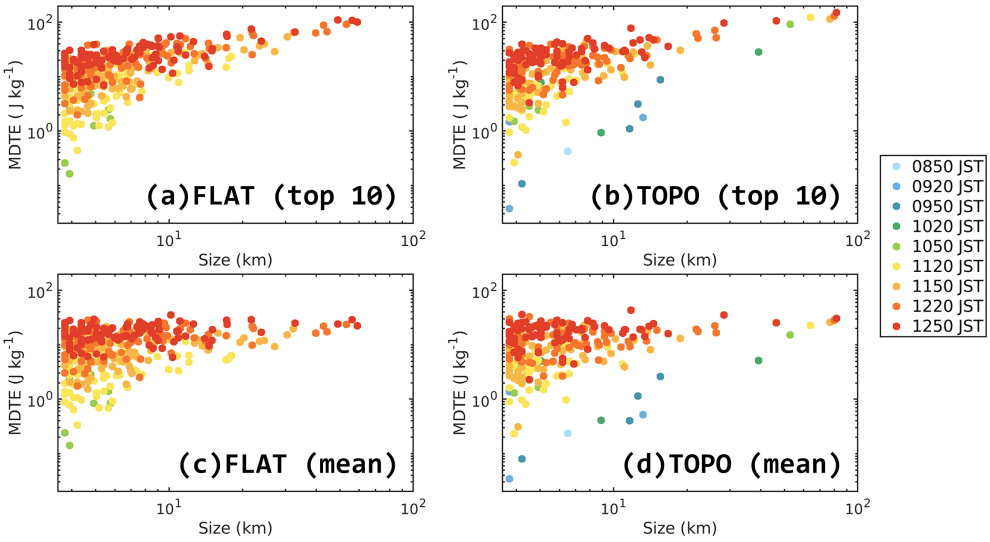

Fig. 6. Scatter plot of the convective cloud size against (a), (b) the mean of maximum 10 MDTE, and (c), (d) the mean MDTE of all grids over the cloud areas detected from (a), (c) FLAT and (b), (d) TOPO. Each point represents a detected cloud area at a time which is represented by color; the x-axis is its size and the y-axis is the MDTE in that cloud area.

of development. This demonstrates the effect of topography on decreasing the nonlinearity of the atmosphere and the associated error growth, not only in the absence of moist convection (recall the decrease of MDTE in Fig. 4) but also when moist convection is occurring.

4. Summary and discussion

The identical twin experiments with and without topography are conducted with the WRF model in an idealized framework to investigate the impact of topography on the initial error growth associated with moist convection. The simulations show clear diurnal cycles and successfully capture the process of the development of afternoon thunderstorm.

In the identical twin experiments, the difference between the control and perturbed simulations is regarded as the error. To estimate the differences between the two simulations, moist difference total energy (MDTE) is calculated. The rapid error growth is triggered by the nonlinearity when the moist convection develops, thus the horizontal spatial distribution, temporal evolution, and the power spectra in wavenumber space of the MDTE is highly related to the development of moist convection. Specifically, the convection in the experiment with topography (TOPO) starts to develop earlier over the mountain and organizes to a larger size. This makes the rapid growth of MDTE over the mountain area occur earliest, and the spectral peak of MDTE propagates to a larger scale at about 20 km. In contrast, the MDTE of the experiment without topography (FLAT) starts the rapid growth at a later time, and its spectra show a characteristic scale of the individual convection cell at about 5 km.

The different features of the convection development between the two experiments greatly dominate the performance of the MDTE. Therefore, the MDTE is also calculated over individual cloud areas at different times to avoid the impact on the MDTE caused by the different convection development. The scatter plot of the cloud size and MDTE suggests that when the convective clouds size is larger, the error could reach a greater magnitude. In addition, for the convective clouds with similar size, those developing over the mountain area lead to smaller MDTE in their early stage of development. This suggests that topography could decrease the rapid error growth introduced by the nonlinearity of moist convection. In other words, it implies that the existence of topography may be able to increase the intrinsic predictability of rapidly developing moist convection like afternoon thunderstorm.

In general, the diurnal cycle of moist convection associated with topography can be seen in various places in the world at various spatial scales (e.g., Romatschke and Houze 2010; Kerns et al. 2010; Takemi 2014), especially under synoptically undisturbed conditions in the warm season. Such diurnal cycle could trigger severe thunderstorms, leading to local sudden heavy rainfall or destructive strong wind. This study identified the topographic effects on the reduction of error growth associated with such thunderstorms, which is scientifically and practically important. Specifically, despite the rapid initial error growth due to the high nonlinearity of moist convection, our results imply that the existence of the topography could decrease the nonlinearity of the system and the following error growth. The effect may come from the forcing of the mountain-induced ascending motion, and convection then develops according to the forcing, which decreases the uncertainty of the convection occurrence. Although a relatively idealized configuration including the topography is used in this study, an actual condition could be more complex. The behavior of the diurnal cycle of moist convection over topography could be affected by different factors such as the environment condition (e.g., Lin et al. 2011) or the orientation of topography and sea breeze (e.g., Kuo and Wu 2019). The findings of this study need to be further investigated with different topography sizes, wind profiles, or atmospheric instability in future studies.

Acknowledgements

This study is supported by JSPS Kakenhi 18H01680, 20H00289, and 21H01591.

Edited by: S.-H. Chen

Supplements

Supplement 1: The meaning and implication of the initial error growth associated with moist convection.

Supplement 2: The physics parameterizations used in this study.

Supplement 3: The time series of domain averaged hourly rainfall and surface-air temperature.

Supplement 4: The procedure to calculate power spectra of the MDTE.

References

Bachmann, K., C. Keil, and M. Weissmann, 2019: Impact of radar data assimilation and orography on predictability of deep convection. *Quart. J. Roy. Meteor. Soc.*, **145**, 117−130, doi: 10.1002/qj.3412.

Bachmann, K., C. Keil, G. C. Craig, M. Weissmann, and C. A. Welzbacher, 2020: Predictability of deep convection in idealized and operational forecasts: Effects of radar data assimilation, orography, and synoptic weather regime. *Mon. Wea. Rev.*, **148**, 63−81, doi:10.1175/MWR-D-19-0045.1.

Bierdel, L., T. Selz, and G. C. Craig, 2018: Theoretical aspects of upscale error growth on the mesoscales: Idealized numerical simulations. *Quart. J. Roy. Meteor. Soc.*, **144**, 682−694, doi:10.1002/qj.3236.

Carbone, R. E., J. D. Tuttle, D. A. Ahijevych, and S. B. Trier, 2002: Inferences of predictability associated with warm season precipitation episodes. *J. Atmos. Sci.*, **59**, 2033−2056.

Dowell, D. C., L. J. Wicker, and C. Snyder, 2011: Ensemble Kalman filter assimilation of radar observations of the 8 May 2003 Oklahoma City supercell: Influences of reflectivity observations on storm-scale analyses. *Mon. Wea. Rev.*, **139**, 272−294.

Ehrendorfer, M., R. M. Errico, and K. D. Raeder, 1999: Singular-vector perturbation growth in a primitive equation model with moist physics. *J. Atmos. Sci.*, **56**, 1627−1648, doi: 10.1175/1520-0469(1999)056<1627:SVPGIA>2.0.CO;2.

Houze, R. A., Jr., 2012: Orographic effects on precipitating clouds. *Rev. Geophys.*, **50**, RG1001, doi:10.1029/2011RG000365.

Jou, B. J.-D., 1994: Mountain-originated mesoscale precipitation system in northern Taiwan: A case study of 21 June 1991. *Terr. Atmos. Oceanic Sci.*, **5**, 169−197

Judt, F., 2018: Insights into atmospheric predictability through global convection-permitting model simulations. *J. Atmos. Sci.*, **75**, 1477−1497, doi:10.1175/JAS-D-17-0343.1.

Kerns, B. W. J., Y.-L. Chen, and M.-Y. Chang, 2010: The diurnal cycle of winds, rain, and clouds over Taiwan during the Mei-Yu, summer, and autumn rainfall regimes. *Mon. Wea. Rev.*, **138**, 497−516.

Kuo, K.-T., and C.-M. Wu, 2019: The precipitation hotspots of afternoon thunderstorms over the Taipei Basin: Idealized numerical simulations. *J. Meteor. Soc. Japan*, **97**, 501−517.

Lin, P.-F., P.-L. Chang, B. J.-D. Jou, J. W. Wilson, and R. D. Roberts, 2011: Warm season afternoon thunderstorm characteristics under weak synoptic-scale forcing over Taiwan Island. *Wea. Forecasting*, **26**, 44−60.

Ngan, K., and G. E. Eperon, 2011: Middle atmosphere predictability in a numerical weather prediction model: Revisiting the inverse error cascade. *Quart. J. Roy. Meteor. Soc.*, **138**, 1366−1378.

Nielsen, E. R., and R. S. Schumacher, 2016: Using convection-allowing ensembles to understand the predictability of an extreme rainfall event. *Mon. Wea. Rev.*, **144**, 3651−3676, doi:10.1175/mwr-d-16-0083.1.

Romatschke, U., and R. A. Houze, Jr., 2010: Extreme summer convection in South America. *J. Climate*, **23**, 3761−3791, doi:10.1175/2010JCLI3465.1.

Selz, T., and G. C. Craig, 2015: Upscale error growth in a high-resolution simulation of a summertime weather event over Europe. *Mon. Wea. Rev.*, **143**, 813−827, doi:10.1175/MWR-D-14-00140.1.

Skamarock, W. C., and co-authors, 2019: *A Description of the Advanced Research WRF Model Version 4*. No. NCAR/TN-556+STR, 145 pp., http://dx.doi.org/10.5065/1dfh-6p97.

Sun, Y. Q., and F. Zhang, 2016: Intrinsic versus practical limits of atmospheric predictability and the significance of the butterfly effect. *J. Atmos. Sci.*, **73**, 1419−1438, doi:10.1175/jas-d-15-0142.1.

Takemi, T., 2014: Characteristics of summertime afternoon rainfall and its environmental conditions in and around the Nobi Plain. *SOLA*, **10**, 158−162, doi:10.2151/sola.2014-033.

Weyn, J. A., and D. R. Durran, 2017: The dependence of the predictability of mesoscale convective systems on the horizontal scale and amplitude of initial errors in idealized simulations. *J. Atmos. Sci.*, **74**, 2191−2210, doi:10.1175/JAS-D-17-0006.1.

Zhang, F., C. Snyder, and R. Rotunno, 2003: Effects of moist convection on mesoscale predictability. *J. Atmos. Sci.*, **66**, 1944−1961, doi:10.1175/2009JAS2824.1.

Zhang, F., N. Bei, R. Rotunno, C. Snyder, and C. C. Epifanio, 2007: Mesoscale predictability of moist baroclinic waves: Convection-permitting experiments and multistage error growth dynamics. *J. Atmos. Sci.*, **64**, 3579−3594.

Manuscript received 9 March 2021, accepted 8 June 2021
SOLA: *https://www.jstage.jst.go.jp/browse/sola/*